Catalysis Letters (2023) 153:477–492
https://doi.org/10.1007/s10562-022-03999-0

The Strong Interaction Between CuO_x and CeO_2 Nanorods Enhanced Methanol Synthesis Activity for CO_2 Hydrogenation

Lei Kong[1,2] · Yuchen Shi[1,2] · Jiaofei Wang[1,2] · Peng Lv[1,2] · Guangsuo Yu[1,2] · Weiguang Su[1,2]

Received: 3 February 2022 / Accepted: 31 March 2022 / Published online: 11 April 2022

Abstract

The Cu/CeO_2-nanopolyhedrals and pure Cu/CeO_2-nanorods with different sizes were synthesized for CO_2 hydrogenation to methanol. With increasing the percentage composition of CeO_2 nanorods, the surface concentrations of Cu^+, Ce^{3+} and oxygen vacancies were gradually enhanced. However, the amount of surface Cu^+ species and oxygen vacancies would be decreased instead if the size of pure CeO_2 nanorods was too large. The variation tendency of catalytic performance for CO_2 hydrogenation to methanol was well consistent with that of Cu^+ species and oxygen vacancies. Cu/CeO_2 nanorods with small size exhibited the strongest interaction in Cu-CeO_2 interface and the highest methanol production activity among all Cu/CeO_2 nano-catalysts. The small size of CeO_2-nanorods obtained at NaOH concentration of 10 mol/L, hydrothermal temperature of 80 °C and hydrothermal time of 24 h showed the best catalytic performance ($X_{CO2}=5.8\%$, $S_{CH3OH}=92.0\%$, $Y_{CH3OH}=5.3\%$) at 280 °C and 3 MPa. The stronger interaction accelerated the charge transfer between CuO_x species and CeO_2 nanorods, which produced the larger amount of surface Cu^+ species and oxygen vacancies. The synergistic effect between reduced Cu species and oxygen vacancies improved methanol selectivity and was responsible for CO_2 hydrogenation to methanol.

Graphical Abstract

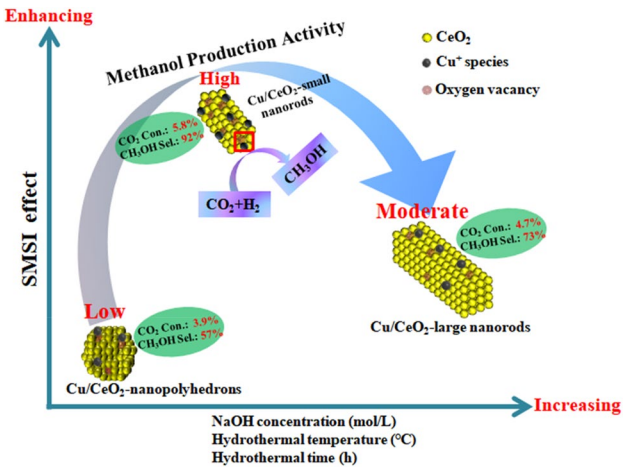

Keywords Cu/CeO_2 nanorods · CO_2 hydrogenation to methanol · Strong interaction · Cu^+ species · Oxygen vacancies

✉ Weiguang Su
weiguangsu@nxu.edu.cn; 63034341@qq.com

[1] State Key Laboratory of High-Efficiency Utilization of Coal and Green Chemical Engineering, Ningxia University, Yinchuan 750021, Ningxia, People's Republic of China

[2] College of Chemistry and Chemical Engineering, Ningxia University, Yinchuan 750021, Ningxia, People's Republic of China

1 Introduction

In recent years, the growing problem of the greenhouse effect resulted from excessive CO_2 emissions has become a major challenge. On the other hand, CO_2 is also a potentially valuable carbon resource in nature, which can be

transformed into high-value chemicals and fuels [1]. Among various CO_2 utilization methods, catalytic synthesis of methanol directly from CO_2 and hydrogen (H_2) holds as a core technology for CO_2 utilization [2]. Methanol is an important solvent and feedstock for the production of chemicals and fuel additives, which is of great significance for the sustainable development of society [3].

Currently, various metal based catalysts have been investigated for the CO_2 hydrogenation to methanol, including Pd, Cu, Au, Pt, Ag supported on different oxides such as ZnO, ZrO_2, TiO_2, CeO_2 etc. [4]. In_2O_3 is also emerging as an active and cost-effective catalyst for methanol synthesis. Among them, some catalysts such as 5Pd5ZnCeO$_2$ [5], 10Au/(3ZnO-ZrO$_2$) [6] and In_2O_3/ZrO_2 [7] have shown 100% selectivity to methanol. However, considering the practical sustainable development and economic benefits, the copper-based catalysts remain an attractive target in the methanol synthesis. CeO_2 is one of the most important oxides in heterogeneous catalysis mainly due to its facile Ce^{4+}/Ce^{3+} redox cycle. It has been reported that the especial redox properties of CeO_2 can be further adjusted by combining with precious and base metal, particularly with copper [8–10]. For the last few years, the application of ceria to form a Cu-CeO_2 system has been highly attempted for CO_2 hydrogenation for methanol [11–15]. In particular, the morphology of CeO_2 has been discovered to have an important role in CO_2 hydrogenation to methanol. The reason is that the crystal planes exposed by CeO_2 with different morphologies can effect some structure-sensitive catalytic reactions. The oxygen vacancy formation over (110) and (111) planes on CeO_2-nanocubes and CeO_2-nanorods requires lower activation energy than conventional and thermodynamically more stable (111) on CeO_2 polyhedral nanoparticles, which leads to higher catalytic activity in many reactions [16]. Typically, Ouyang et al. [17] studied the morphology dependence of CO_2 hydrogenation to methanol over CeO_2 nanostructures and the results showed that the Cu/CeO_2 nanorods catalysts exposed with (110) and (110) faces exhibited the strongest CuO-CeO_2 interaction and highest CuO dispersion, which resulted in the highest catalytic activity with methanol yield of 1.9%. Similarly, Jiang et al. [18] found that Pd/CeO_2-Rods by the exposure of (110) and (111) facets showed the lowest oxygen vacancy formation energy and the highest density as well as the most amount of surface oxygen vacancies for methanol synthesis. They attributed the superiority to the influence of surface structure and morphology of ceria. Furthermore, Tan et al. [19] demonstrated that CeO_2 nanorod-supported Cu-Ni alloy exposed with more (100) and (110) facets and numerous oxygen vacancies, which has exhibited more superior catalytic performance for methanol synthesis than on CeO_2 nanospheres and nanoparticles. Xie et al. [20] prepared a serious of Co/$CeO_{2\text{-}6}$ catalysts with different morphology structure for CO_2 catalytic hydrogenation reaction. The results showed that the different morphology structure of CeO_2 support obviously influence the exposed crystal plane. The exposed (110) and (100) crystal plane of CoCe140 catalyst nano-rods exhibited the excellent CO_2 hydrogenation performance.

As is well-known, the catalytic activities of many nanocatalysts have been strongly dependent on their sizes and morphologies in heterogeneous [21–23]. To date, the morphology-controlled synthesis of CeO_2 supports has been studied as an effective strategy to prepare promising Cu/CeO_2 catalysts for CO_2 hydrogenation to methanol. Nevertheless, the systematic and comprehensive study of the nanoscale size-determined catalytic performance of CeO_2 nanostructures needs to be further demonstrated. Recently, some reports have revealed the relationship between the size of CeO_2 supports and heterogeneous catalytic performance. For example, Dong et al. [24] showed that the catalytic properties of the CeO_2 nanocubes for CO oxidation exhibited a prominent size effect, the conversion of CO increased as the size of the CeO_2 nanocubes reduced. Lagarashi et al. [25] found that the calytic performance in dehydration of butanediol was greatly affected by the particle size of CeO_2, the selectivity to unsaturated alcohols enhanced with increasing the particle size. However, to the best of our knowledge, how the size of CeO_2 nanomaterials affects the performance of catalysts for the CO_2 hydrogenation to methanol is rarely investigated up to now, particularly the size of CeO_2 nanorods. In this work, a series of CeO_2 supporters with different morphology and size were synthesized, but the exposed crystal facets were almost the same. Cu/CeO_2 nanorods with small size showed the strongest interaction in Cu-CeO_2 interface and the highest formation rate of methanol. It was proposed that the strongest interaction between CuO_x species and CeO_2 was beneficial to generating more reduced Cu species and oxygen vacancies. The synergistic effect between reduced Cu species and oxygen vacancies greatly promoted the formation of methanol.

2 Experimental

2.1 Catalyst Preparation

All of the chemicals in our experiments were of analytical grade and used without further purification. Cerium nitrate hexahydrate (99.5%) was obtained from Shanghai Macklin Biochemical Technology Co., Ltd (Shanghai, China). Copper (II) nitrate trihydrate (99.0%) and sodium hydroxide (96.0%) were purchased from Shanghai WoKai Biotechnology Co., Ltd (Shanghai, China).

2.1.1 CeO_2 Preparation

In a typical synthesis, 3.2 mmol Ce(NO3)3·6H2O was dissolved in deionized water (10 mL) to produce a transparent solution, different masses of NaOH was dissolved in deionized water (54 mL) to make the NaOH concentrations at 1, 4, 10 and 12 mol/L, then NaOH solution was added into the Ce(NO3)3 solution to prepare a suspension mixture. After being stirred at room temperature for 30 min, the mixture was transferred into a 100 mL Teflon-lined stainless autoclave and heated at 60, 80 and 100℃ for 12, 24 and 36 h, respectively. After the reaction, autoclave was cooled to room temperature naturally and fresh products were collected by centrifugation, washed with deionized water to neutrality. The CeO_2 nanostructures were obtained by drying at 80 °C overnight, and then were calcined at 450 °C for 5 h in air to produce yellowish ceria powder.

2.1.2 Cu/CeO_2 Preparation

The Cu/CeO_2 catalysts were prepared by deposition–precipitation method. 0.5 g of CeO_2 support and 0.33 g Cu $(NO_3)_2{\cdot}3H_2O$ were dispersed in 30 mL of deionized water to reach the desired nominal copper loading (15 wt%). Then 0.83 g urea was added to the above mentioned dispersion to ensure uniform copper hydroxycarbonate precipitation on the CeO_2 surface. The molar ratio of urea to Cu $(NO_3)_2{\cdot}3H_2O$ was 10. The above mixture was stirred and reacted at 90 °C for 18 h. Then the resulting suspension was centrifuged, dried overnight and finally calcined in air at 400 °C for 4 h.

2.2 Catalyst Characterization

Powder X-ray diffraction (XRD) patterns of the samples were recorded on a Bruker D8 Advance diffractometer with Cu Kα radiation source operated at 40 kV and 40 mA. Bragger's angles were scanned in the range of 2θ between 20 and 80 degree. The average crystallite sizes were estimated from the Scherrer's equation.

Transmission electron microscopy (TEM) measurements were operated on a FEI Tecnai G^2 F20 transmission electron microscope at 200 kV. The samples were suspended in ethanol solution using an ultrasonic bath for 0.5 h. One drop of the suspension was cast on a copper grid for the TEM sample preparation.

X-ray photoelectron spectroscopy (XPS) measurements were performed on a Thermo Scientific K-Alpha spectrometer with a monochromatic Al Kα (1486.6 eV) radiation source. During data processing of XPS spectra, the charging shift was calibrated using C 1 s value of adventitious carbon at binding energy 284.8 eV.

Brunauer-Eemmet-Teller (BET) surface area and pore volume of the samples were determined by measuring N_2 adsorption–desorption isotherms at liquid nitrogen temperature (−196 °C) using a Micromeritics ASAP 2460 adsorption apparatus. The samples were degassed under a vacuum of 10^{-5} Torr for 12 h at 200 °C.

H_2 temperature-programmed reduction (TPR) was conducted on a Micromeritics Apparauts (AutoChem II 2920) to examine the redox behavior of the samples. The gas was 10% H_2/Ar mixture and the flow rate of gas was 50 mL/min. 40 mg sample was placed on top of some silica wool in a quartz reactor. Before reduction, the sample was pretreated at 300 °C for 1 h in a He stream in order to remove the contaminants, and then it was cooled to room temperature. The H_2/Ar mixture was switched on and the sample was heated with a heating rate of 10 °C/min. The reduction reaction was performed from room temperature to 900 °C.

2.3 Evaluation of Catalyst Activity

The catalytic activity was tested in a continuous fixed bed quartz tube reactor (d_{int}, 8 mm) packed with 0.1 g of catalyst (40–80 mesh). Before the reaction test, the loaded catalyst was pre-reduced under a 20% H_2/N_2 mixture gas flow (40 mL/min) at 0.1 MPa and 300 °C for 1 h. After reduction, the catalyst bed was cooled to initial reaction temperature (220 °C) and then purged with the reactant gas (V_{CO2}: V_{H2} = 1:3). The gas hourly space velocity (GHSV) was fixed at 24,000 mL/h/g. Then, the reactor was pressurized to 3 MPa using the reactant gas and maintained for 4 h to reach a steady state. The reactor was heated to the desired temperature (220–450 °C), and the temperature ramp to the next measuring point was 20 °C. Then the isothermal and isobaric conditions were maintained for 2 h at each reaction temperature for product analysis. The lines between the reactor and the gas chromatograph were heated to 160 °C to avoid the condensation of methanol as well as other high boiling point product. The remaining reactant CO_2 and by product CO were analyzed by an on-line gas chromatograph (Agilent 7890B) equipped with TCD detector. Methanol and other hydrocarbons were analyzed using FID detector (Agilent 7890B). The CO_2 conversion (X_{CO2}), product selectivities (S_{CO}, S_{CH4}, and S_{CH3OH}) were defined using the following equations.

$$X_{CO_2} = \frac{n_{CH_3OH} + n_{CO} + n_{CH_4} + 2n_{C_2H_5OH}}{n_{CO_2} + n_{CH_3OH} + n_{CO} + n_{CH_4} + 2n_{C_2H_5OH}} \times 100\%$$

$$= \frac{F_{CH_3OH} \times A_{CH_3OH} + F_{CO} \times A_{CO} + F_{CH_4} \times A_{CH_4} + 2F_{C_2H_5OH} \times A_{C_2H_5OH}}{FCO_2 \times A_{CO_2} + F_{CH_3OH} \times A_{CH_3OH} + F_{CO} \times A_{CO} + F_{CH_4} \times A_{CH_4} + 2F_{C_2H_5OH} \times A_{C_2H_5OH}} \times 100\%$$

$$S_{CH_3OH} = \frac{n_{CH_3OH}}{n_{CH_3OH} + n_{CO} + n_{CH_4} + 2n_{C_2H_5OH}} \times 100\%$$

$$= \frac{F_{CH_3OH} \times A_{CH_3OH}}{F_{CH_3OH} \times A_{CH_3OH} + F_{CO} \times A_{CO} + F_{CH_4} \times A_{CH_4} + 2F_{C_2H_5OH} \times A_{C_2H_5OH}} \times 100\%$$

$$S_{CH_4} = \frac{n_{CH_4}}{n_{CH_3OH} + n_{CO} + n_{CH_4} + 2n_{C_2H_5OH}} \times 100\%$$

$$= \frac{F_{CH_4} \times A_{CH_4}}{F_{CH_3OH} \times A_{CH_3OH} + F_{CO} \times A_{CO} + F_{CH_4} \times A_{CH_4} + 2F_{C_2H_5OH} \times A_{C_2H_5OH}} \times 100\%$$

$$S_{CO} = \frac{n_{CO}}{n_{CH_3OH} + n_{CO} + n_{CH_4} + 2n_{C_2H_5OH}} \times 100\%$$

$$= \frac{F_{CO} \times A_{CO}}{F_{CH_3OH} \times A_{CH_3OH} + F_{CO} \times A_{CO} + F_{CH_4} \times A_{CH_4} + 2F_{C_2H_5OH} \times A_{C_2H_5OH}} \times 100\%$$

F is the relative correction factor. $F_{CO_2} = 1$. A is the peak area.

3 Results and Discussion

3.1 Textural and Structural Properties of Cu/CeO_2

Figure 1a showed the XRD patterns of the Cu/CeO_2 catalysts obtained at different concentration of NaOH. Diffraction peaks at 2θ of 28.6°, 33.1°, 47.5°, 56.3°, 59.1°, 69.4°, 76.7° and 79.1° were assigned to the (111), (200), (220), (311), (222), (400), (331), and (420) crystal planes of face-centered cubic structure CeO_2 (space group Fm3m) reported in JCPDS Card (PDF#34–0394) [26]. Only two weak peaks at 35.6° and 38.7° could be indexed to the (002) and (111) planes of CuO (PDF#45–0937). The small and weak reflection peaks for CuO indicated that CuO was highly dispersed on the surface of CeO_2 supports. Furthermore, when the concentration of NaOH increased from 1 to 12 mol/L, the intensity of CuO diffraction peaks was almost the same, indicating that the crystalline size of CuO was hardly changed. However, the diffraction peaks of CeO_2 became sharp with the increasing concentration of NaOH, suggesting that the size and crystallinity of CeO_2 gradually got larger and better. As shown in Table 1, the average crystalline sizes of CeO_2 estimated according to the Scherrer's equation were 9.2, 9.6, 13.4 and 14.5 nm in Cu/CeO_2−1 mol/L, Cu/CeO_2−4 mol/L, Cu/CeO_2−10 mol/L and Cu/CeO_2−12 mol/L, respectively. XRD patterns of Cu/CeO_2 prepared at different hydrothermal temperatures were displayed in Fig. 1b. The results were similar to those shown in Fig. 1a. No changes were observed in the diffraction peaks of CuO in Cu/CeO_2−60 °C, Cu/CeO_2−80 °C and Cu/CeO_2−100 °C, illustrating that the crystalline size of CuO did not change with the increase of hydrothermal temperature. It could be seen that the intensity of CeO_2 crystal phase peaks enhanced with increasing hydrothermal temperature. The average crystallinity size of CeO_2 in Cu/CeO_2−60 °C, Cu/CeO_2−80 °C and Cu/CeO_2−100 °C was 8.0, 8.6 and 12.7 nm, respectively. XRD patterns of Cu/CeO_2 catalysts prepared with different hydrothermal time were also shown in Fig. 1c. Similarly, the diffraction peaks corresponding to CuO phases were weak and almost unchanged with increasing hydrothermal time, while the intensity of CeO_2 diffraction peaks was gradually increased. The crystallinity sizes of CeO_2 in Cu/CeO_2−12 h, Cu/CeO_2-24−h and Cu/CeO_2−36 h were 8.5, 8.6 and 9.1 nm, respectively. XRD results indicated that the crystalline sizes of CeO_2 were gradually increased with enhancing NaOH concentration, hydrothermal temperature and hydrothermal time, while the sizes of CuO remained nearly constant. Moreover, the exposed crystal facets of CeO_2 were also hardly changed.

TEM observations were performed on all the samples in order to explore their morphology and particle size. Figure 2 displayed the TEM images of Cu/CeO_2 catalysts prepared with different concentrations of NaOH. The hydrothermal temperature and hydrothermal time were fixed at 100 °C and 24 h, respectively. As shown in Fig. 2a, mountains

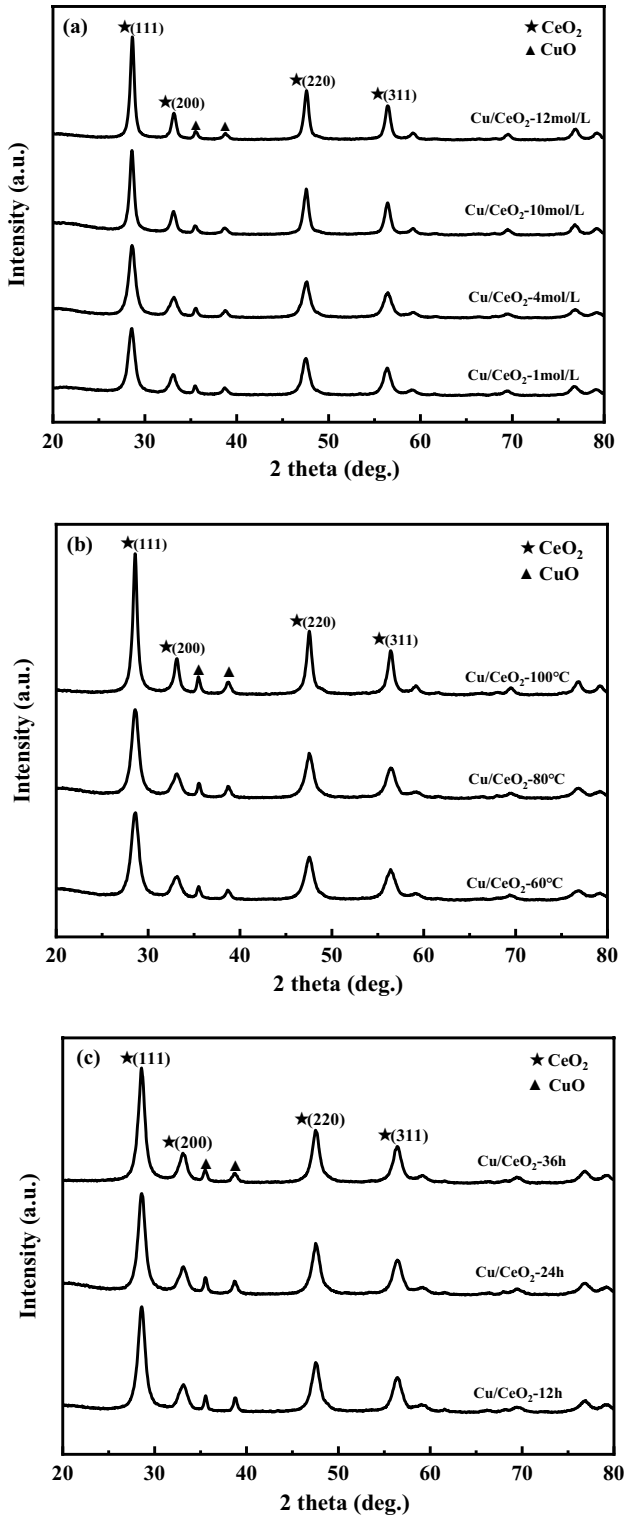

Fig. 1 XRD patterns of Cu/CeO_2 catalysts obtained under **a** different concentrations of NaOH at 100 °C hydrothermal temperature and 24 h hydrothermal times, **b** different hydrothermal temperatures at 10 mol/L NaOH concentrations and 24 h hydrothermal times, and **c** different hydrothermal times at 10 mol/L NaOH concentrations and 100 °C hydrothermal temperature

Table 1 Structural property of Cu/CeO_2 catalysts prepared at different hydrothermal synthesis conditions

Catalyst	CeO_2 cell Parameter (nm)	Crystalline Size (nm)	S_{BET} (m^2/g)	Pore volume (cm^3/g)
Cu/ CeO_2-1 mol/L	0.5411	9.2	48.7	0.13
Cu/ CeO_2-4 mol/L	0.5411	9.3	55.1	0.16
Cu/CeO_2- 10 mol/L	0.5411	13.4	58.2	0.19
Cu/CeO_2- 12 mol/L	0.5411	14.5	77.7	0.24
Cu/CeO_2-60 °C	0.5411	8.0	83.2	0.25
Cu/CeO_2-80 °C	0.5411	8.6	89.8	0.23
Cu/CeO_2-100 °C	0.5411	13.4	58.2	0.19
Cu/CeO_2-12 h	0.5411	8.5	76.5	0.21
Cu/CeO_2-24 h	0.5411	8.6	89.8	0.23
Cu/CeO_2-36 h	0.5411	9.1	81.7	0.22

of nanopolyhedrals and a small quantity of nanorods were observed when the concentration of NaOH was 1 mol/L. The length of nanorods changed from 20 to 60 nm, and the diameters of nanorods changed from 6 to 8 nm. The diameter of nanopolyhedrals was about 6–12 nm. The morphology of CeO_2 was composed of abundant nanopolyhedrals and a little amount of nanorods. Compared with Fig. 2a, when the concentration of NaOH increased to 4 mol/L, a large number of CeO_2 nanopolyhedrals have been transformed into nanorods and the nanorods featured 8–12 nm in diameter and 50–150 nm in length (Fig. 2b), suggesting that the higher concentration of NaOH was more conducive to the formation of CeO_2 nanorods. The CeO_2 nanopolyhedrals were completely transformed into uniform nanorods and only CeO_2 nanorods were observed when the concentration of NaOH reached 10 mol/L. At the moment, the length of nanorods ranged from 60 to 240 nm and the diameter ranged from 9 to 15 nm (Fig. 2c). Both the length and diameter of nanorods got bigger when the concentration of NaOH was further increased to 12 mol/L. The CeO_2 nanorods exhibited a wider diameter distribution of 10–21 nm and a longer length between 120 and 300 nm (Fig. 2d). It could be also seen that the spherical CuO nanoparticles were dispersed on the surface of CeO_2, and the average size of CuO nanopariticles was relatively uniform and about 5–7 nm. With the increase of NaOH concentrations, CeO_2 nanopolyhedrals were gradually transformed to CeO_2 nanorods and the size of CeO_2 nanorods became larger, while the size of spherical CuO nanoparticles was almost unchanged.

Figure 3 showed the morphology and size of CeO_2 prepared at different hydrothermal temperatures. The concentration of NaOH and hydrothermal time were 10 mol/L and 24 h, respectively. The Cu/CeO_2 obtained at 60 °C in

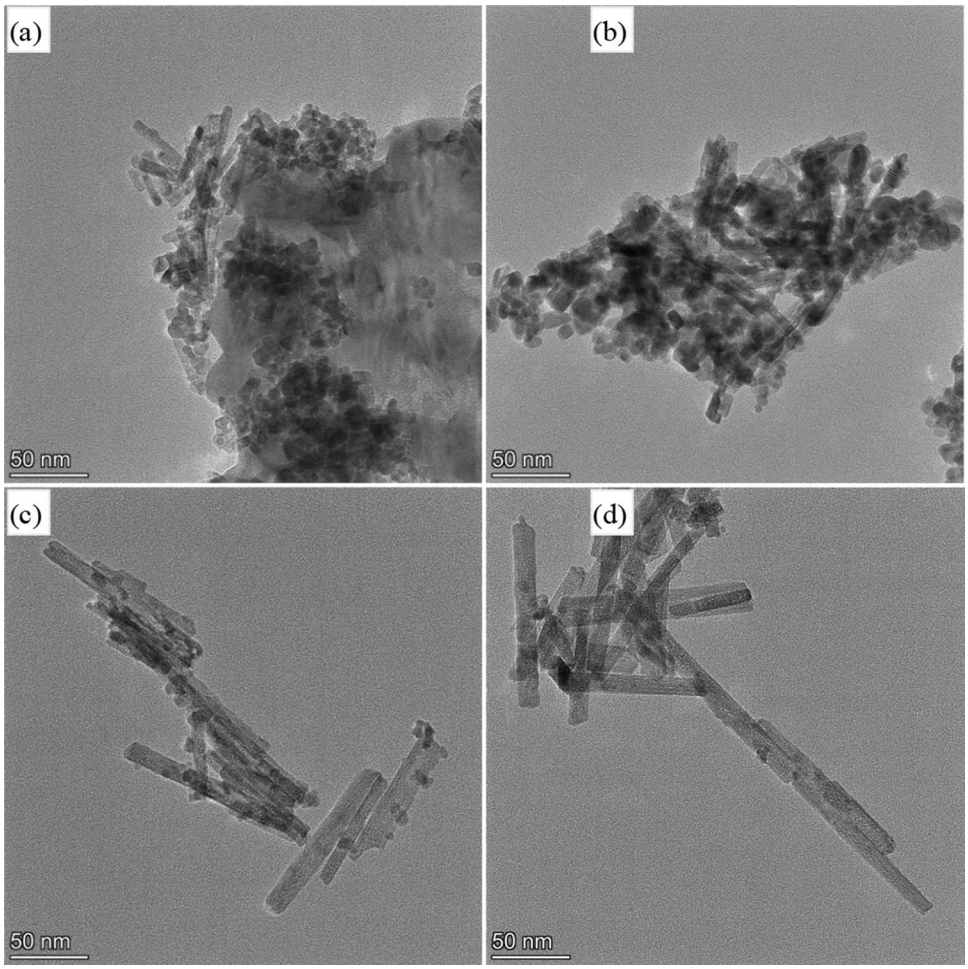

Fig. 2 TEM images of Cu/CeO_2 catalysts obtained at 100 °C hydrothermal temperature and 24 h hydrothermal times with different concentrations of NaOH. **a** 1 mol/L, **b** 4 mol/L, **c** 10 mol/L, and **d** 12 mol/L

Fig. 3a exhibited a semblable morphology with the Cu/CeO_2−4 mol/L (Fig. 2b), which consisted of nanorods of 5–7 nm in diameter and 30–50 nm in length and nanopolyhedrals of about 5–11 nm in diameter. After increasing the hydrothermal temperature to 80 °C, only uniform CeO_2 nanorods were formed. The diameter and length of nanorods grew to 6–13 and 90–200 nm (Fig. 3b). When the hydrothermal temperature was enhanced to 100 °C, the average diameter and length of CeO_2 nanorods were further increased to 10–25 and 100–450 nm, respectively. However, the size of CuO nanoparticles was still maintained at about 5–7 nm when the hydrothermal temperature was ranged from 60 °C to 100 °C. Compared with the concentration of NaOH, the effect of hydrothermal temperature on the morphology and size of CeO_2 was more obvious.

Figure 4 indicated the TEM images of Cu/CeO_2 catalysts obtained at different hydrothermal time. The concentration of NaOH and hydrothermal temperature were 10 mol/L and 80 °C. Likewise, Cu/CeO_2 obtained at 12 h in Fig. 4a displayed the similar morphology with Cu/CeO_2−1 mol/L (Fig. 2a) and Cu/CeO_2−60 °C (Fig. 3a), which was made up of nanoparticles with diameter of 7–14 nm and nanorods with diameter of 4–8 nm and length of 30–80 nm. When the hydrothermal time was increased to 24 and 36 h, the homogeneous CeO_2 nanorods were fully formed, the diameter and length of nanorods were 6–13 and 90–200 nm (Fig. 4b), 8–14 and 100–300 nm (Fig. 4c), respectively. However, the average size of CuO nanoparticles remained unchanged at about 5–7 nm. As mentioned above, increasing the concentrations of NaOH or hydrothermal temperature or hydrothermal time was favorable to the transformation of CeO_2 nanopolyhedrals into nanorods, and the size of CeO_2 nanorods was also gradually increased. The results of TEM were in good agreement with those of XRD.

The N_2 adsorption–desorption isothermal plots of Cu/CeO_2 catalysts obtained under different concentrations of NaOH, different hydrothermal temperatures, and different hydrothermal times were shown in Figure S1a, S1b and S1c, respectively. The isotherms of all samples were of classical type IV as defined by Brunauer-Deming-Deming-Teller (BDDT) pore model [27], which was characteristic of mesoporous materials due to the textural of inter-particle mesoporosity. All the samples exhibited type H3 hysteresis loops in the relative pressure (P/P_0) range from 0.6 to 1.0.

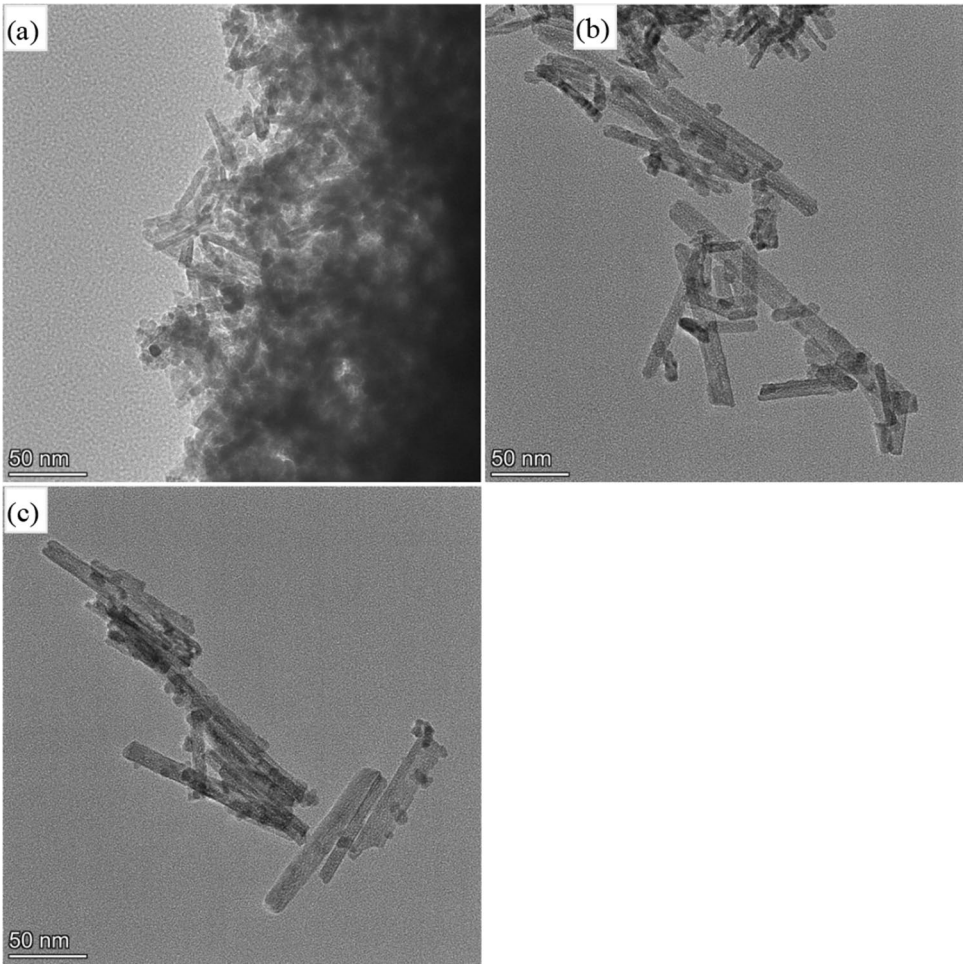

Fig. 3 TEM images of Cu/CeO_2 catalysts obtained at 10 mol/L NaOH concentrations and 24 h hydrothermal times under different hydrothermal temperatures. **a** 60 °C, **b** 80 °C, and **c** 100 °C

This H3-type of the hysteresis loop was typical for wormhole-like mesostructure and interstice mesoporous structure formed by nanoparticle assembly [28]. Moreover, as seen in Table 1, it could be seen that the BET surface area increased gradually with the increase of NaOH concentrations. However, with the increase of hydrothermal temperature and hydrothermal time, BET surface area firstly increased and then decreased. Large BET surface area was favorable for oxygen storage capacity (OSC) of ceria because OSC taken place not only on the surface but also in the bulk. Therefore, combining with the TEM images, it was evident that the morphologies and sizes of ceria had a great influence on the BET surface area of catalysts.

The pore size distribution curves of all the samples determined by the BJH method. As shown in Figure S2a, the adsorption branch of the corresponding isotherm of Cu/CeO_2−1 mol/L and Cu/CeO_2−4 mol/L exhibited one relative widely peak centered at 6.7 and 12.2 nm, but Cu/CeO_2−10 mol/L and Cu/CeO_2−12 mol/L exhibited a narrow peak centered at 2.2 and 2.4 nm and another wide peak centered at 29.6 and 27.9 nm, indicating th at the mesopore distribution of the samples became more uneven with the increase of NaOH concentration. Similarly, as shown in Figure S2b, the BJH pore size distribution plots of the samples obtained at different hydrothermal temperature exhibited a nonuniform mesopore size distribution with the increase hydrothermal temperature. However, the pore size distribution curves of the samples prepared at different hydrothermal times showed these catalysts possessed uniform mespore size distributions shown in Figure S2c.

3.2 Surface Chemical Properties of Cu/CeO_2

XPS measurement was performed to analyze the surface composition and elementary oxidation states of the Cu/CeO_2 catalysts. Figure 5 showed the related XPS spectra (Cu2p, Ce3d and O1s) of Cu/CeO_2 obtained with different concentrations of NaOH. As shown in Fig. 5a, there were two characteristic peaks for $Cu2p_{3/2}$, the main peak at ~ 932.5 eV was attributed to the binding energy of Cu^+ species and the weak peak at ~ 934.7 eV was assigned to the binding energy of Cu^{2+} species [29]. The existence of plenty of Cu^+ species should be mainly due to the redox cycle of $Cu^{2+} + Ce^{3+} \leftrightarrow Cu^+ + Ce^{4+}$ [30]. Previously, some reports

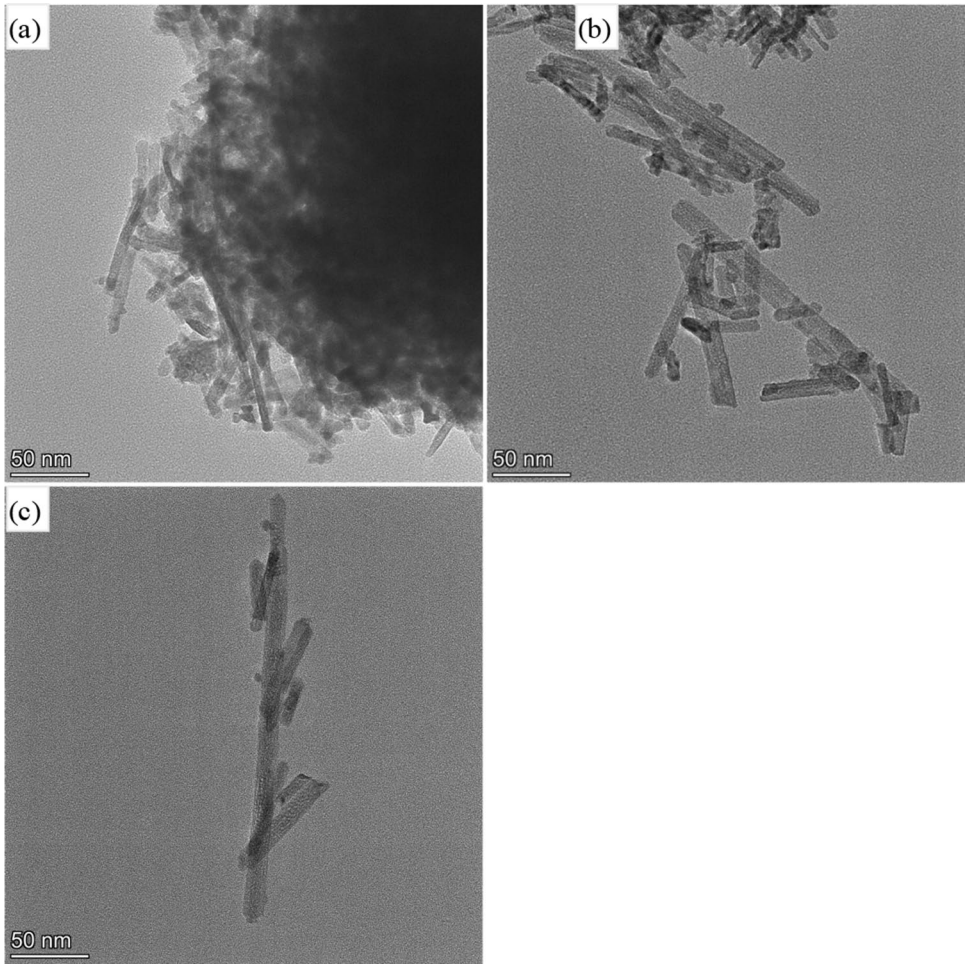

Fig. 4 TEM images of Cu/CeO_2 catalysts obtained at 10 mol/L NaOH concentrations and 100 °C hydrothermal temperature under different hydrothermal times. **a** 12 h, **b** 24 h, and **c** 36 h

proposed that the reaction of CO_2 hydrogenation to methanol took place on the Cu-CeO_2 interface, and the electrons could transfer readily between copper and ceria, which resulted in Cu^+ and Ce^{3+} species formation [31]. The surface atomic ratios of $Cu^+/(Cu^{2+}+Cu^+)$ were calculated via a semiquantitative analysis and listed in Table 2. As shown in Table 2, Cu/CeO_2-1 mol/L exhibited a minimum proportion of Cu^+ species which was 64%. When the concentration of NaOH reached to 4 mol/L, the proportion of Cu^+ increased to 76%. After the concentration of NaOH was further increased to 10 and 12 mol/L, the content of Cu^+ species remained almost unchanged at about 86%. Combined with XRD and TEM results, the different Cu^+ content maybe originate from the morphology of the CeO_2 supports. It was clear that the content of surface Cu^+ species was gradually increased with the elevation of the proportion of nanorods in CeO_2 supports, suggesting that the CeO_2 nanorods were more conductive to the formation of Cu^+ species. It was probably implied that there was a more facile redox cycle between copper and ceria nanorods comparing with CeO_2 nanopolyhedrals.

XPS spectra of Ce3d were numerically resolved into eight peaks for each sample after deconvolution, and the corresponding assignments were defined in Fig. 5b. The Ce3d spectra were composed of two-group spin orbitals of overlapping peaks labeled as U (U-U''') for $3d_{3/2}$ and V (V-V''') for $3d_{5/2}$. It was widely reported that the peaks of U' (903.0 eV) and V' (884.2 eV) were attributed to Ce^{3+}, and the other six peaks corresponded to Ce^{4+} [31]. As a result, the surface of CeO_2 was mainly in a + 4 oxidation state and a small part of Ce^{3+} co-existed. The surface amount of Ce^{3+} shown as $Ce^{3+}/(Ce^{3+}+Ce^{4+})$ in Table 2, could be estimated by considering the relative integrated areas of the corresponding peaks and the total Ce 3d region [32–34]. As shown in Table 2, the surface content of Ce^{3+} rose gradually with increasing NaOH concentration. The variation trend of surface concentration of Ce^{3+} species was consistent with that of surface Cu^+ species (Table 2). Thus, according to the TEM and XPS results, it could be concluded that the CeO_2 nanorods were more advantageous to form the surface Ce^{3+}, and Ce^{3+} species promoted the formation of Cu^+ species. In addition, according to the charge compensation principle, the presence of Ce^{3+} was closely associated with the generation of oxygen vacancies. It meant that the transformation process of Ce^{4+} to Ce^{3+} brought about the formation

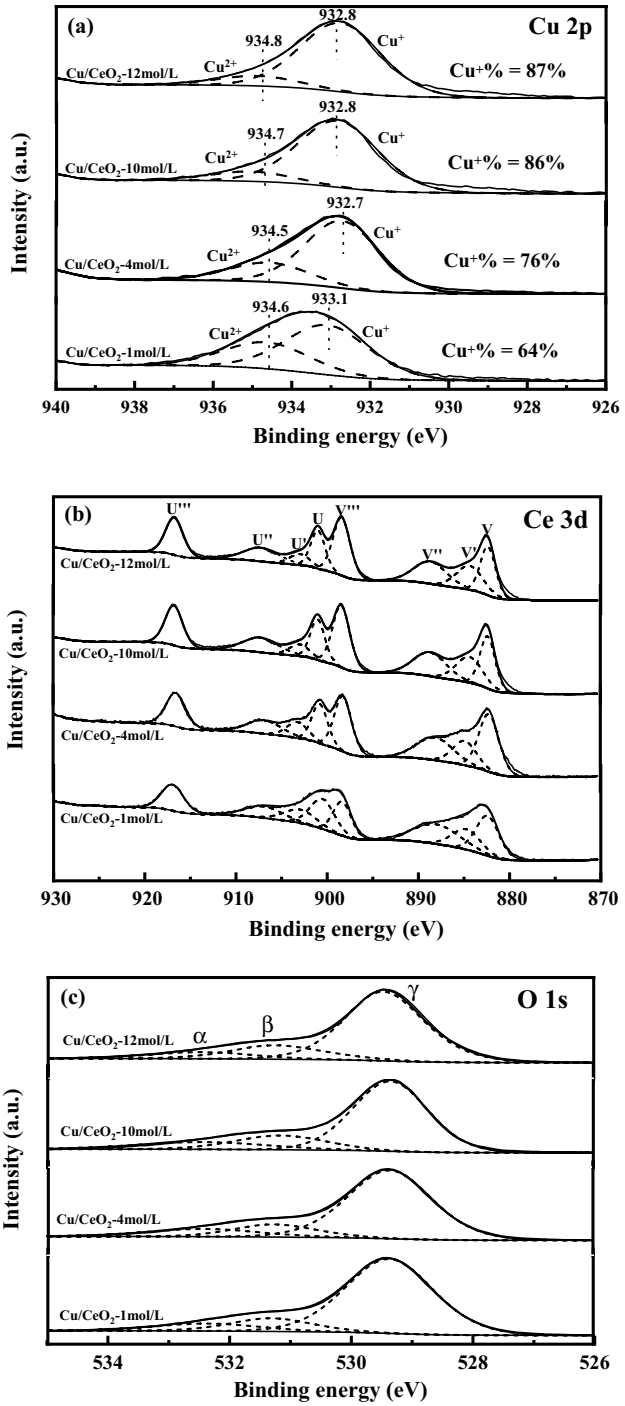

Fig. 5 **a** Cu2p XPS spectra, **b** Ce3d XPS spectra, and **c** O1s XPS spectra of Cu/CeO_2 catalysts obtained at 100 °C hydrothermal temperature and 24 h hydrothermal times with different concentrations of NaOH

of oxygen vacancies in Cu/CeO_2. Those oxygen vacancies were considered to be active and play an important role in CO_2 hydrogenation to methanol [35]. It was demonstrated that the CeO_2 nanorods with small size had a better ability

Table 2 Surface element composition calculated by XPS

Catalyst	Surface element composition (%)		
	$Cu^+/(Cu^+ + Cu^{2+})$	$Ce^{3+}/(Ce^{3+} + Ce^{4+})$	$(\alpha+\beta)/(\alpha+\beta+\gamma)$
Cu/CeO_2-1 mol/L	64	15	22
Cu/CeO_2-4 mol/L	76	15	25
Cu/CeO_2-10 mol/L	86	16	30
Cu/CeO_2-12 mol/L	87	17	30
Cu/CeO_2-60 °C	87	11	19
Cu/CeO_2-80 °C	90	15	38
Cu/CeO_2-100 °C	86	16	30
Cu/CeO_2-12 h	78	11	25
Cu/CeO_2-24 h	90	15	38
Cu/CeO_2-36 h	86	12	34

to transform the electron between copper and ceria and form more oxygen vacancies.

Figure 5c indicated the O1s spectra of Cu/CeO_2 synthesized with different concentration of NaOH, where two states of surface oxygen species existed. The peak at ~ 529.3 eV (γ) could be attributed to lattice oxygen, and the other two peaks were assigned to defect oxygen species, including chemisorbed oxygen species (~ 531.3 eV, β) and hydroxyl-like groups (~ 532.1 eV, α) [36]. The ratios of $(\alpha+\beta)/(\alpha+\beta+\gamma)$ for Cu/CeO_2 shown in Table 2 were used to evaluate the concentration of the oxygen vacancies. It was apparent that the $(\alpha+\beta)/(\alpha+\beta+\gamma)$ ratio ranked in the following order: Cu/CeO_2−10 mol/L (30%) > Cu/CeO_2−12 mol/L (26%) > Cu/CeO_2−4 mol/L (25%) > Cu/CeO_2−1 mol/L (20%), which was basically consistent with the variation trend of Ce^{3+} and Cu^+ content. Herein, it could be concluded that the surface chemical state of Cu/CeO_2 catalysts was significantly affected by the morphology of CeO_2 supports. CeO_2 nanorods possessed the higher Cu^+, Ce^{3+} and oxygen vacancy concentration comparing with CeO_2 nanopolyhedrals.

The typical XPS spectra of Cu2p, Ce3d and O1s binding energies of Cu/CeO_2 catalysts obtained at different hydrothermal temperatures were shown in Fig. 6. The estimated percent content of Cu^+ species were shown in Table 2. Among three catalysts, Cu/CeO_2−80 °C exhibited the highest Cu^+ content (90%), followed by Cu/CeO_2−60 °C (87%) and Cu/CeO_2−100 °C (86%). In addition, as shown in Table 2, both Ce^{3+} and oxygen vacancy concentration of Cu/CeO_2−80 °C were highest compared with Cu/CeO_2−60 °C and Cu/CeO_2−100 °C, which were 15% and 38%, respectively. TEM results showed that the Cu/CeO_2−60 °C was composed of CeO_2 nanorods and CeO_2 nanopolyhedrals. Both Cu/CeO_2−80 °C and Cu/CeO_2−100 °C were

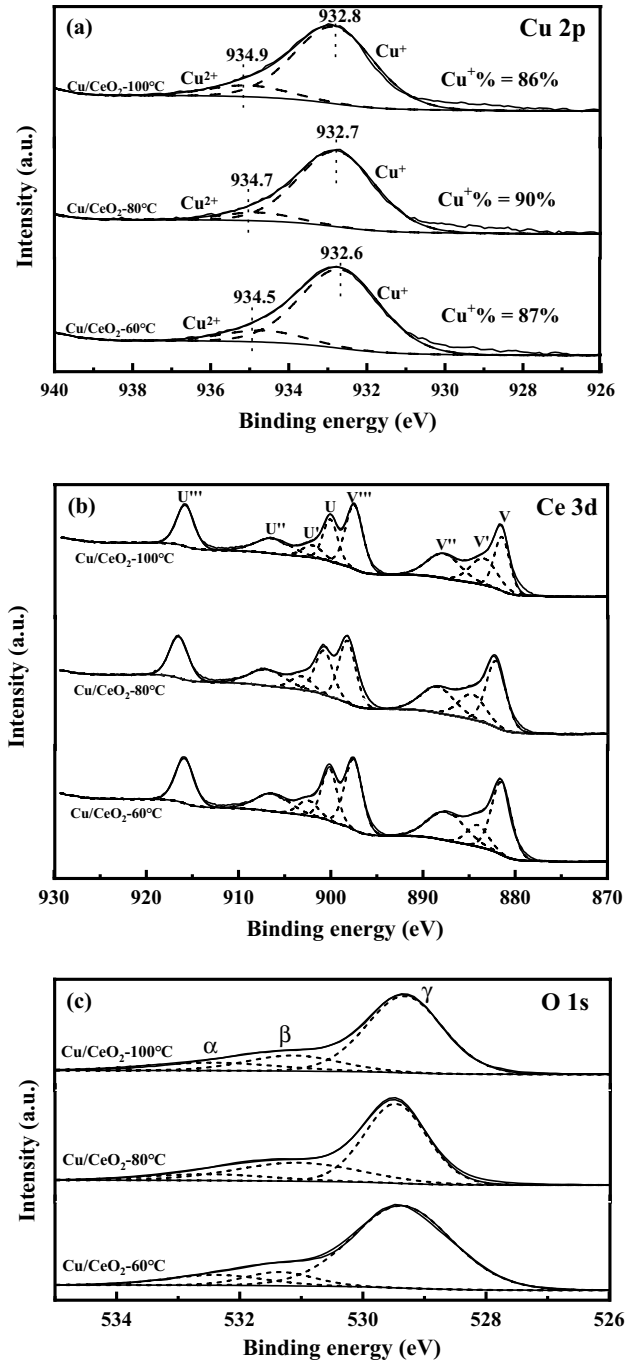

Fig. 6 **a** Cu2p XPS spectra, **b** Ce3d XPS spectra, and **c** O1s XPS spectra of Cu/CeO_2 catalysts obtained at 10 mol/L NaOH concentrations and 24 h hydrothermal times under different hydrothermal temperatures

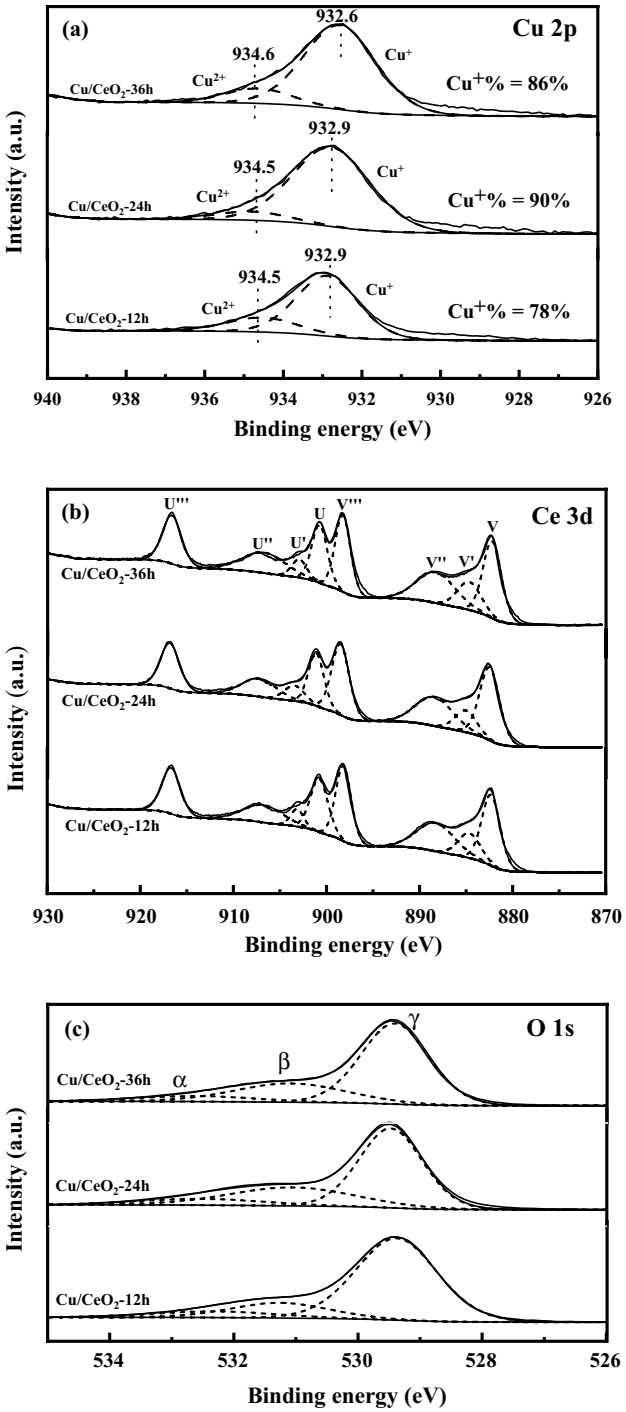

Fig. 7 **a** Cu2p XPS spectra, **b** Ce3d XPS spectra, and **c** O1s XPS spectra of Cu/CeO_2 catalysts obtained at 10 mol/L NaOH concentrations and 100 °C hydrothermal temperature under different hydrothermal times

all CeO_2 nanorods, but the size of CeO_2 nanorods in Cu/CeO_2−100 °C was much larger than that in Cu/CeO_2−80 °C, suggesting that CeO_2 nanorods with larger size was also not conducive to the formation of oxygen vacancies. Thus, it was proposed that the CeO_2 nanorods with small size had higher proportion of Ce^{3+} concentration, which could result in more formation of Cu^+ species and oxygen vacancies. Namely, Cu/CeO_2−80 °C catalyst exhibited the strongest interaction between copper and ceria.

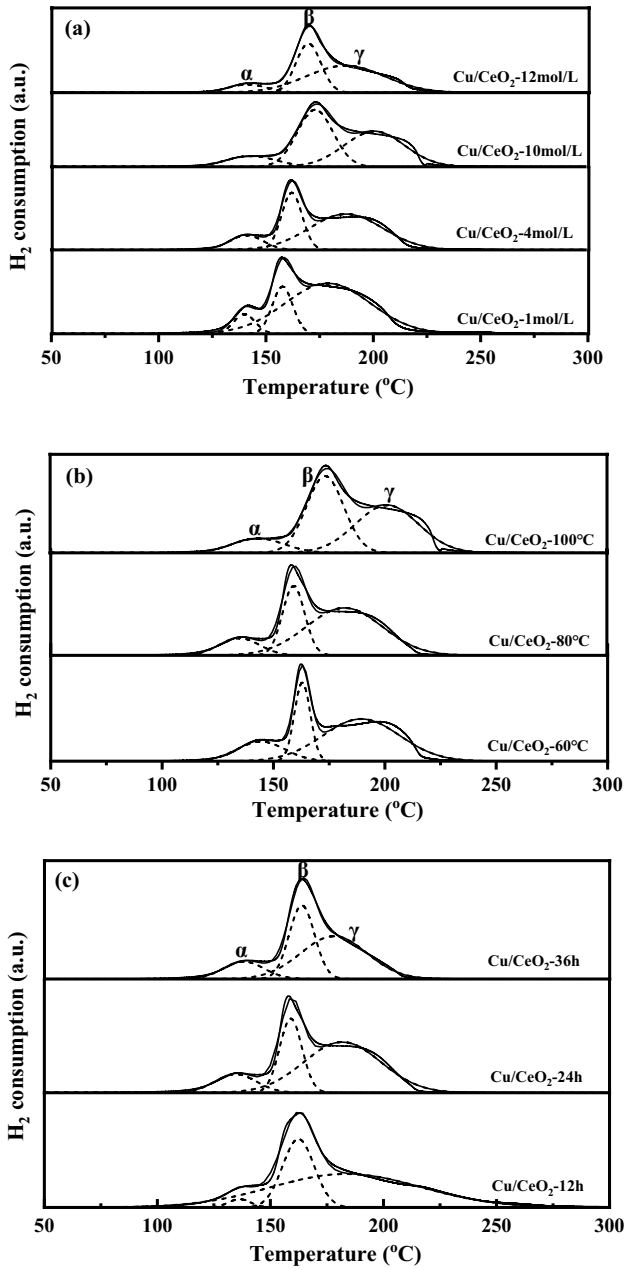

Fig. 8 H_2-TPR profiles of Cu/CeO_2 catalysts obtained under **a**different concentrations of NaOH at 100 °C hydrothermal temperature and 24 h hydrothermal times, **b** different hydrothermal temperatures at 10 mol/L NaOH concentrations and 24 h hydrothermal times, and **c** different hydrothermal times at 10 mol/L NaOH concentrations and 100 °C hydrothermal temperature

Figure 7 displayed the corresponding Cu2p, Ce3d and O1s XPS spectra of Cu/CeO_2 obtained at different hydrothermal time. The calculated percent content of Cu^+, Ce^{3+} species and oxygen vacancy for Cu/CeO_2 catalysts were summarized in Table 2. A highest Cu^+ content was found in the Cu/CeO_2−24 h (90%), while the content of Cu^+ species was about 78% and 86% in Cu/CeO_2−12 h and Cu/CeO_2−36 h, respectively. Meanwhile, both the calculated percent content of Ce^{3+} and oxygen vacancies followed the order: Cu/CeO_2-24 h > Cu/CeO_2-36 h > Cu/CeO_2-12 h. Combining with TEM results, hydrothermal temperature and hydrothermal time had a significant effect on the morphology of CeO_2 and the size of CeO_2 nanorods. In summary, comparing with CeO_2 nanopolyhedrals and CeO_2 nanorods with larger size, it was indicated that CeO_2 nanorods with small size (diameter ranging from 8 to 15 nm and length ranging from 100 to 200 nm) exhibited the stronger electron transfer capability and the more formation of Cu^+ species and oxygen vacancies.

H_2-TPR measurements were used to investigate the reduction of Cu/CeO_2 catalysts and the interaction between copper and ceria. The H_2-TPR profiles of Cu/CeO_2 prepared at different concentration of NaOH, different hydrothermal temperature and different hydrothermal time were shown in Fig. 8 and the temperature of reduction peak and H_2 consumption were listed in Table 3. The hydrogen reduction peaks of all Cu/CeO_2 catalysts could be deconvoluted into three Gaussian peaks denoting as α, β and γ, which were located at about 140, 165 and 200 °C, respectively. The three peaks were attributed to the reduction of the highly dispersed CuO_x species which interacted strongly with the ceria, the reduction of CuO_x species which interacted weakly with the ceria and the reduction of bulk CuO [37], respectively. The strong interaction between CuO_x and ceria (peak α) was considered to have a largely positive effect on the CO_2 hydrogenation catalytic activity over the supported Cu/CeO_2 catalyst, and the interaction between copper oxide and CeO_2 was proven to promote the reduction of copper oxide to Cu^+ [38]. The stronger the interaction was, the lower the reduction temperature would result. According to the above TEM results, it was known that CeO_2 nanopolyhedrals would be gradually changed to CeO_2 nanorods and the size of CeO_2 nanorods also grew bigger with increasing the concentrations of NaOH or hydrothermal temperature or hydrothermal time. As shown in Fig. 8 and Table 3, with increasing the percentage content of CeO_2 nanorods, the reduction peaks especially the α peak shifted towards low temperature, but the total amount of H_2 consumption was enhanced. The Cu/CeO_2−80 °C catalyst with pure CeO_2 nanorods exhibited a lowest reduction temperature of peak α at 134 °C and a highest H_2 consumption total amount of 2.02 mmol/g, indicating Cu/CeO_2−80 °C possessed the strongest interaction between copper oxide and CeO_2. However, it was worth noting that the reduction temperature of CuO_x species was increased and H_2 consumption amount was decreased instead if the size of CeO_2 nanorods further rising. It was revealed that CeO_2 nanorods with small size could promote the dispersion and reducibility of the surface CuO_x species. The interaction between copper oxide and CeO_2 nanorods was much stronger than that between copper oxide and CeO_2 nanopolyhedrals,

Table 3 Reduction temperature and H_2 consumption amount of Cu/CeO_2 catalysts summarized in H_2-TPR

Reduction temperature and H_2 consumption amount							
Catalyst	Total (mmol/g)	Peak α		Peak β		Peak γ	
		T (°C)	Area (%)	T (°C)	Area (%)	T (°C)	Area (%)
Cu/CeO_2-1 mol/L	1.48	142	0.11 (7.4%)	157	0.25 (16.9%)	189	1.12 (75.7%)
Cu/CeO_2-4 mol/L	1.52	141	0.18 (12.0%)	162	0.41 (27.3%)	197	0.93 (61.2%)
Cu/CeO_2-10 mol/L	2.01	139	0.23 (11.3%)	174	0.87 (43.4%)	210	0.91 (45.3%)
Cu/CeO_2-12 mol/L	2.02	141	0.17 (8.6%)	170	0.68 (33.5%)	207	1.17 (57.9%)
Cu/CeO_2-60 °C	1.74	144	0.30 (17.2%)	162	0.40 (23.0%)	198	1.04 (59.8%)
Cu/CeO_2-80 °C	2.02	134	0.24 (12.0%)	159	0.54 (26.8%)	182	1.24 (61.1%)
Cu/CeO_2-100 °C	2.01	139	0.23 (11.3%)	174	0.87 (43.4%)	210	0.91 (45.8%)
Cu/CeO_2-12 h	1.83	136	0.05 (2.5%)	162	0.54 (29.3%)	183	1.25 (68.2%)
Cu/CeO_2-24 h	2.02	134	0.24 (12.0%)	159	0.54 (26.8%)	182	1.24 (61.1%)
Cu/CeO_2-36 h	1.69	138	0.22 (13.1%)	164	0.59 (34.7%)	178	0.88 (52.2%)

but the large CeO_2 nanorods would weaken this interaction. The strong interaction accelerated the charge transfer rate between CuO_x species and CeO_2 nanorods, which was beneficial to the reduction and good dispersion of CuO_x species on CeO_2 surface. The results of H_2-TPR were in good accordance with XPS results.

3.3 Catalytic Performance

Figure 9a indicated the methanol selectivity as a function of CO_2 conversion over Cu/CeO_2 catalysts obtained at different concentration of NaOH. It could be seen that the methanol selectivity decreased monotonously with the increase of CO_2 conversion for all Cu/CeO_2 catalysts. For the Cu/CeO_2−1 mol/L catalyst, the methanol selectivity was about 78% with CO_2 conversion of 2.2% at the reaction temperature of 260 °C. With increasing the concentration of NaOH, the methanol production activity was gradually enhanced and methanol selectivity reached the highest at the similar level of CO_2 conversion when NaOH concentration was 10 mol/L. At the reaction temperature of 280 °C, 86% methanol selectivity could still be achieved when the CO_2 conversion was 2.8%. Nevertheless, the selectivity towards methanol started to decline instead with further increasing the concentration of NaOH. When NaOH concentration was increased to 12 mol/L, methanol selectivity was decreased to 84% at the CO_2 conversion of 2.6%.

In order to investigate the effect of hydrothermal temperature on catalytic performance of CO_2 hydrothermal to methanol, the methanol selectivity as a function of CO_2 conversion over Cu/CeO_2 catalysts prepared under different hydrothermal temperatures was carried out in Fig. 9b. With increasing the hydrothermal temperature, methanol production activity was first increased and then decreased. The methanol formation rate reached the maximum when the hydrothermal temperature was 80 °C, and 92% methanol selectivity could still be achieved even the CO_2 conversion reached up to 5.8% at the reaction temperature of 320 °C. By contrast, only 57% methanol selectivity was obtained even CO_2 conversion was as low as 3.9% when the hydrothermal temperature was 60 °C. Further increasing the hydrothermal temperature, the methanol formation rate began to decrease instead. The selectivity to methanol was decreased to 73% at the CO_2 conversion of 4.7% when the hydrothermal temperature was enhanced to 100 °C.

Figure 9c also displayed the catalytic performance of CO_2 hydrogenation to methanol over Cu/CeO_2 catalysts prepared at different hydrothermal time. Similarly, the activity of CO_2 hydrogenation to methanol first increased and then decreased with the increase of hydrothermal time. The highest methanol selectivity was obtained on Cu/CeO_2 synthesized under a hydrothermal time of 24 h. For example, when CO_2 conversion was about 5%, Cu/CeO_2−24 h presented a methanol selectivity of 93%, whereas the selectivity to methanol on Cu/CeO_2−12 h and Cu/CeO_2−36 h was only 68% and 40%, respectively. The variation trend of methanol formation rate with increasing NaOH concentration, hydrothermal temperature and hydrothermal time was nearly consistent.

3.4 Discussion

It was widely known that nano-catalysts with high surface area provided abundant active sites for the adsorption and activation of reactant, thus exhibited better catalytic activity. As shown in Table 1, the Cu/CeO_2−10 mol/L catalyst showed a much lower surface area of only 58.2 m^2/g, but exhibited a very higher catalytic activity for CO_2

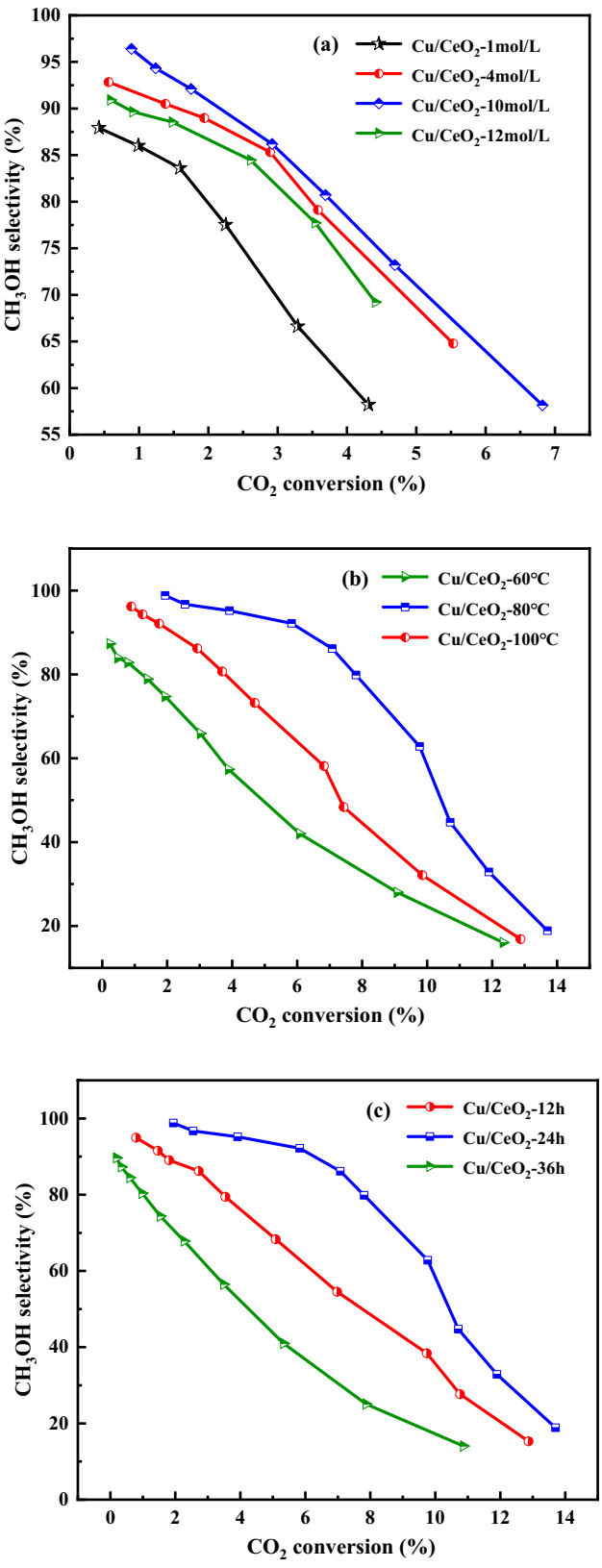

Fig. 9 Methanol selectivity as a function of CO_2 conversion on Cu/CeO_2 catalysts obtained under **a** different concentrations of NaOH at 100 °C hydrothermal temperature and 24 h hydrothermal times, **b** different hydrothermal temperatures at 10 mol/L NaOH concentrations and 24 h hydrothermal times, and **c** different hydrothermal times at 10 mol/L NaOH concentrations and 100 °C hydrothermal temperature. Reaction conditions: catalyst mass, 0.1 g; CO_2: H_2 = 1: 3; reaction temperature: 220–410 °C; reaction pressure: 3 MPa; space velocity: 24,000 mL/g/h

hydrogenation to methanol. Thus, it was deduced that the surface area played role in the performance of catalysts, but not the main factor. In addition, TEM results indicated that the CuO particle size was always maintained at about 5–7 nm under different hydrothermal synthesis conditions and XRD results showed that the exposed crystal facets of CeO_2 were nearly the same. Therefore, it could be also inferred that the CuO particle size and crystal facets of CeO_2 worked on catalytic performance, but were not the influencing factor accountable for CO_2 hydrogenation to methanol in this work. On the basis of the above characterization results, it could be deduced that the morphology and size of CeO_2 supports played a significant role in both CO_2 conversion and methanol selectivity of Cu/CeO_2 catalysts for CO_2 hydrogenation.

According to the above TEM results and catalytic activities for methanol synthesis, as the proportion of nanorods in the CeO_2 carriers increased, both the selectivity and formation rate of methanol on Cu/CeO_2 catalysts were gradually enhanced, indicating that the Cu/CeO_2 nanorods were more beneficial to the production of methanol than Cu/CeO_2 nanopolyhedrals. Nevertheless, the CeO_2 nanorods with too large size would inhibit the formation of methanol. Combined with the XPS results, the Cu/CeO_2 nanorods catalysts were more likely to form surface Cu^+ species than Cu/CeO_2 nanopolyhedrals. On the other hand, it was apparent that the variation trend of methanol production activity was completely consistent with the variation trend of Cu^+ concentration, demonstrating that the Cu^+ species was a key factor in determining methanol production. It was speculated that the Cu^+ species might be the active sites for CO_2 hydrogenation to methanol. The above results were in good accordance with some literature reports. In the presence of CO_2 and a large fraction of Cu^0 surface covered by oxygen-containing species, Chinchen et al. [39] found that the catalytic activity toward methanol synthesis was independent of the Cu^0 surface area. They considered that the Cu^+ sites might be acting as the active sites in methanol synthesis. On the basis of apparent activation energy measurements, X-ray photoelectron spectroscopy and scanning electron microscopy results, Sheffer and King [40] demonstrated that different activity toward methanol synthesis among unsupported copper catalysts promoted by group IA elements could be attributed to the different concentration of Cu^+ species. Van Santen et al.

Table 4 Comparison of the obtained performance on CO_2 hydrogenation to methanol with previous published works

Catalyst	Space velocity	T_R (°C)	P_R (°C)	X_{CO2} (%)	S_{CH3OH} (%)	References
5%Cu/CeO_2-NR	3000 (W)	280	3	3.3	38.9	[17]
5%Cu/CeO_2-NC	3000 (W)	280	3	2.8	46.2	[17]
5%Pd/CeO_2-NR	60,000 (G)	260	5	7.3	74.9	[45]
5%Pd/CeO_2-NC	60,000 (G)	260	5	6.5	68.5	[45]
0.92 In-4.6Cu/CeO_2	7200 (W)	210	3	7.6	95.0	[46]
1Pd-10Cu/CeO_2	–	230	3	14.8	29.0	[47]
1Cu2Ni/CeO_2-NR	6000 (G)	260	3	18.4	73.3	[19]
Au/CeO_2	20,000 (G)	225	–	2.1	62.2	[48]
5Pd5ZnCeO_2	2400 (W)	220	3	6.3	100	[5]
Pd/CeO_2-500	–	230	3	3.1	91.7	[49]
15%Cu/CeO_2-small NR	24,000 (W)	280	3	5.8	92.0	This work

[41] stated that anything else that stabilizing the presence of Cu^+ indiscriminately enhanced the methanol production activity. In contrast to CeO_2 nanopolyhedrals, the results of H_2-TPR indicated that CuO_x species supported on CeO_2 nanorods had lower reduction temperature and was more easily reduced. It was suggested that the pure CeO_2 nanorods with small size exhibited stronger interaction between copper and ceria, which was more beneficial to the generation of Cu^+. The stronger interaction in Cu-CeO_2 interface would cause the facile electron transfer between copper and ceria, which led to the transformation of Ce^{4+} to Ce^{3+} and the formation of Cu^+ species [13, 42]. More recently, according to the high-pressure in situ DRIFTS results, Yu et al. [43] proposed that the promotional effect of Cu^+ on the stabilization of CO^* intermediates, which inhibited CO desorption and facilitates further hydrogenation to CH_3OH via the RWGS + CO-Hydro pathway. Thus, due to the strong interaction between CuO_x and CeO_2 as well as high CuO_x dispersion, Cu/CeO_2 nanorods with small size exhibited the highest concentration of Cu^+ species, which greatly stabilized adsorbed CO^* intermediates and promoted the methanol formation. In addition, the transformation of Ce^{4+} to Ce^{3+} brought the charge imbalance and the formation of oxygen vacancies on the surface of Cu/CeO_2 nanorods [44]. These oxygen vacancies were also considered to be active and played an important role in CO_2 hydrogenation to methanol [36].Correspondingly, as shown in Table 2, the significantly improved methanol synthesis activity of Cu/CeO_2-80 °C with the largest number of oxygen vacancies was possibly attributed to the strongest electron transfer rate between copper and CeO_2 nanorods with small size, which was crucial for enhancing the activity of CO_2 hydrogenation to methanol.

Hence, based on the above experiment results, it was conclude that the synergistic effect between reduced Cu species and oxygen vacancies was accountable for CO_2 hydrogenation to methanol. Furthermore, the better dispersion of CuO_x species on the surface of CeO_2 nanorods ware also in favor of producing methanol. In this work, the Cu-CeO_2 nanorods obtained at NaOH concentration of 10 mol/L, hydrothermal temperature of 80 °C and hydrothermal time of 24 h showed the best catalytic performance (X_{CO2} = 5.8%, S_{CH3OH} = 92.0%, Y_{CH3OH} = 5.3%) at 280 °C and 3 MPa. As shown in Table 4, this result was close to the Pd/CeO_2-nanorods catalyst synthesized by the wet impregnation method reported by Khobragade et al. [45]. The superior methanol production activity reached a higher level in contrast to the results reported in the literature, indicating that Cu/CeO_2 nanorods with small size was a potential and excellent catalyst for CO_2 hydrogenation to methanol.

4 Conclusions

The CeO_2-nanopolyhedrals and CeO_2-nanorods with different sizes were synthesized via different hydrothermal synthesis conditions, and Cu/CeO_2 catalysts were prepared by a deposition–precipitation method for CO_2 hydrogenation to methanol. With increasing the NaOH concentration or hydrothermal temperature or hydrothermal time, CeO_2 nanopolyhedrals were gradually transformed into CeO_2 nanorods and the size of CeO_2 nanorods became larger. The variation trends of the surface concentration of Cu^+, Ce^{3+} and oxygen vacancies were in good agreement. CeO_2 nanorods with small size supported Cu/CeO_2 had the maximum amount of surface Cu^+ species and oxygen vacancies. Comparing with CeO_2 nanopolyhedrals, the pure Cu/CeO_2 nanorods catalyst exhibited the lower reduction temperature of CuO_x species and greater H_2 consumption amount, indicating the stronger interaction in Cu-CeO_2 nanorods interface and better dispersion of CuO_x species. Accordingly, the methanol synthesis activity for CO_2 hydrogenation on Cu/CeO_2 nanorods was much higher than that on Cu/CeO_2 nanopolyhedrals. The Cu-CeO_2 nanorods with small size obtained at NaOH concentration of 10 mol/L, hydrothermal temperature of 80 °C and hydrothermal time of 24 h showed the best catalytic

performance (X_{CO2} = 5.8%, S_{CH3OH} = 92.0%, Y_{CH3OH} = 5.3%) at 280 °C and 3 MPa. The CeO_2 nanorods with small size had a stronger interaction between CuO_x species and ceria to form higher concentration of surface Cu^+ species and more oxygen vacancies, which provided more active sites and dramatically promoted the formation rate of methanol for CO_2 hydrogenation.

Supplementary Information The online version contains supplementary material available at https://doi.org/10.1007/s10562-022-03999-0.

Acknowledgements This work was financially supported by the National Natural Science Foundation of China (No. 21463018) and the Key Research and Development Project of Ningxia Province (The Western Light, No. 201709).

Declarations

Conflict of Interest The author declare that they have no known competing financial interests or personal relationships that could have appeared to influence the work reported in this paper.

References

1. Li S-Z, Wang Y, Yang B, Guo L-M (2019) A highly active and selective mesostructured Cu/AlCeO catalyst for CO_2 hydrogenation to methanol. Appl Catal A 571:51–60
2. Dang S-S, Yang H-Y, Gao P, Wang H, Li X-P, Wei W, Sun Y-H (2019) A review of research progress on heterogeneous catalysts for methanol synthesis from carbon dioxide hydrogenation. Catal Today 330:61–75
3. Zhou W, Cheng K, Kang J-C, Zhou C, Subramanian V, Zhang Q-H, Wang Y (2019) New horizon in C1 chemistry: breaking the selectivity limitation transformation of syngas and hydrogenation of CO_2 into hydrocarbon chemicals and fuels. Chem Soc Rev 48:3193–9228
4. Zhong J-W, Yang X-F, Wu Z-L, Liang B-L, Huang Y-Q, Zhang T (2020) State of the art and perspective in heterogeneous catalysis of CO_2 hydrogenation to methanol. Chem Soc Rev 49:1385–1413
5. Malik A-S, Zaman S-F, Al-Zahrani A-A, Daous M-A, Driss H, Petrov L-A (2018) Development of highly selective PdZn/CeO_2 and Ga-doped PdZn/CeO_2 catalysts for methanol synthesis from CO_2 hydrogenation. Appl Catal A 560:42–53
6. Sloczynski J, Grabowski R, Kozlowska A, Olszewski P, Stoch J, Skrzypek J, Lachowska M (2004) Catalytic activity of the M/($3ZnO{\cdot}ZrO_2$) system (M=Cu, Ag, Au) in the hydrogenation of CO_2 to methanol. Appl Catal A 278:11–23
7. Martin O, Martin D-A-J, Mondelli D-C, Mitchell D-S (2016) Indium oxides as a superior catalyst for methanol synthesis by CO_2 hydrogenation. Angew Chem Int Edit 55:6261–6265
8. Beckers J, Rothenberg G (2010) Sustainable selective oxidation using ceria-based materials. Green Chem 12:939
9. Acerbi N, Tsang S-C-E, Jones G, Golunski S, Collier P (2013) Rationalization of interactions in precious metal/ceria catalysts using the d-band center model. Angew Chem Int Ed Engl 52:7737–7741
10. Ganduglia-Pirovano M-V (2015) The non-innocent role of cerium oxide in heterogeneous catalysis: a theoretical perspective. Catal Today 2:1–13
11. Nix R-M, Rayment T, Lambert R-M, Robert Jennings J, Owen J (1987) An in suit X-ray diffraction study of the activation and performance of methanol synthesis catalysts derived from rare earth-copper alloys. J Catal 106:216–234
12. Sripada P, Kimpton J, Barlow A, Williams T, Kandasamy S, Bhattacharya S (2020) Investigating the dynamic structural changes on Cu/CeO_2 catalysts observed during CO_2 hydrogenation. J Catal 381:415–426
13. Graciani J, Mudiyanselage K, Xu F, Baber A-E, Evans J, Senanayake S-D, Stacchiola D-J, Liu P, Hrbek J, Sanz J-F, Rodriguez J-A (2014) Highly active copper-ceria and copper-ceria-titania catalysts for methanol synthesis from CO_2. Science 345:546–550
14. Wang W-W, Qu Z-P, Song L-X, Fu Q (2020) CO_2 hydrogenation to methanol over Cu/CeO_2 and Cu/ZrO_2 catalysts: Turning methanol selectivity via metal-support interaction. J Energy Chem 40:22–30
15. Varvoutis G, Lykaki M, Papis E (2021) Effect of alkali (Cs) doping on the surface chemistry and CO_2 hydrogenation performance of CuO/CeO_2 catalysts. J CO2 Util 44:101408–101416
16. Moretti E, Lenarda M, Storaro L, Talon A (2007) Catalytic purification of hydrogen streams by PROX on Cu supported on an organized mesoporous ceria-modified alumina. Appl Catal B: Environ 72:149–156
17. Ouyang B, Tan W-L, Liu B (2017) Morphology effect of nanostructure ceria on the Cu/CeO_2 catalysts for synthesis of methanol from CO_2 hydrogenation. Catal Commun 95:36–39
18. Jiang F, Wang S-S, Liu B, Liu J, Wang L, Xiao Y, Xu Y-B, Liu X-H (2020) Insights into the influence of CeO_2 crystal facet on CO_2 hydrogenation to methanol over Pd/CeO_2 catalysts. ACS Catal 10:11493–11509
19. Tan Q-Q, Shi Z-S, Wu D-F (2019) CO_2 hydrogenation over differently morphological CeO_2-supported Cu-Ni catalysts. Int J Energy Res 43:5392–5404
20. Xie F-Q, Xu S-Y, Deng L-D, Xie H-M (2020) CO_2 hydrogenation on Co/$CeO_{2\text{-}6}$ catalyst: morphology effect from CeO_2 support. Int J Hydro Ener 45:26938–26952
21. Hartadi Y, Widmann D, Behm J (2015) CO_2 hydrogenation to methanol on supported Aucatalysts under moderate reaction conditions: support and particle size effects. ChemSuschem 8:456–465
22. Sykes E-C-H, Tikhov M-S, Lambert R-M (2002) Quantum size effects in catalysis byTiO_2/Platinum: the switch from partial oxidation to partial hydrogenation of styrene. Catal Lett 82:169–173
23. Bai L-C, Wang X, Chen Q, Ye Y-F, Zheng H-Q, Guo J-H, Yin Y-D, Gao C-B (2016) Explaining the size dependence in platinum-nanoparticle-catalyzed hydrogenation reactions. Angew Chem Int Ed 55:15656–15661
24. Dong C-Y, Zhou Y, Ta N, Shen W-J (2020) Formation mechanism and size control of cerianano cubes. CrystEngComm 22:3033–3041
25. Igarashi A, Ichikawa N, Sato S, Takahashi R, Sodesawa T (2006) Dehydration of butanediolsover CeO_2 catalysts with different particle sizes. Appl Catal A 300:50–57
26. Rajkumar T, Sápi A, Ábel M, Kiss J, Szenti I (2021) Surface engineering of CeO_2 catalysts: differences between solid solution based and interfacially designed $Ce_{1\text{-}x}M_xO_2$ and MO/CeO_2 (M=Zn, Mn) in C_O2 hydrogenation reaction. Catal Lett 151:3477–3491
27. Sing K-S-W, Everett D-H, Haul R-A-W, Moscou L, Pierotti R-A, Rouquerol J, Siemieniewska T (1985) Reporting physisorption data for gas/solid systems with special reference to the determination of surface area and porosity. Pure Appl Chem 57:603–619
28. Cao J-L, Wang Y, Zhang T-Y, Wu S-H, Yuan Z-Y (2008) Preparation, characterization and catalytic behavior of nanostructured mesoporous CuO/$Ce_{0.8}Zr_{0.2}O_2$ catalysts for low-temperature CO oxidation. Appl Catal B 78:120–128

29. Glisenti A, Natile M-M, Carlotto S, Vittadini A (2014) Co- and Cu-doped titanates: toward a new generation of catalytic converters. Catal Lett 144:1466–1471
30. Zabilskiy M, Djinovic P, Pintar A (2015) Nanashaped CuO/CeO_2 materials: effect of the exposed ceria surfaces on catalytic activity in N_2O decomposition reaction. ACS Catal 5:5357–5365
31. He Y-H, Liang X, Chen B-H (2013) Surface selective growth of ceria nanocrystals by CO absorption. Chem Commun 79:9000–9002
32. Xie Y, Wu J-F, Jing G-J, Zhang H (2018) Structural origin of high catalytic activity for preferential CO oxidation over CuO/CeO_2 nanocatalysts with different shapes. Appl Catal B 239:665–676
33. Chen S-Q, Li L-Q, Hu W-B, Huang X-S, Li Q, Xu Y-S, Zuo Y, Li G-S (2015) Anchoring high-concentration oxygen vacancies at interfaces of CeO_{2-x}/Cu toward enhanced activity for preferential CO oxidation. ACS Appl Mater & Inter 7:22999–23007
34. Dongil A-B, Bachiller-Baeza B, Castillejos E, Escalona N (2016) The promoter effect of potassium in CuO/CeO_2 systems supported on carbon nanotubes and graphene for the CO-PROX reaction. Catal Sci Technol 6:6118–6127
35. Guo X-L, Li J, Zhou R-X (2016) Catalytic performance of manganese doped $CuO\text{-}CeO_2$ catalysts for selective oxidation of CO in hydrogen-rich gas. Fuel 163:56–64
36. Bao J, Yang G-H, Yoneyama Y, Tsubaki N (2019) Significant advances in C1 catalysis: highly efficient catalysts and catalytic reactions. ACS Catal 9:3026–3053
37. Wang W-W, Qu Z-P, Song L-X, Fu Q (2020) Probing into the multifunctional role of copper species and reaction pathway on copper-cerium-zirconium catalysts for CO_2 hydrogenation to methanol using high pressure in situ DRIFTS. J Catal 382:129–140
38. Shim J-O, Na H-S, Jha A, Jang W-J, Jeong D-W, Nah I-W, Jeon B-H, Roh H-S (2016) Effect of preparation method on the oxygen vacancy concentration of CeO_2-promoted $Cu/\gamma\text{-}Al_2O_3$ catalysts for HTS reactions. Chem Eng J 306:908–915
39. Li L, Song L, Chen C-Q, Zhang Y-J, Zhan Y-Y, Lin X-Y, Zheng Q, Wang H-D, Ma H-X, Ding L-H, Zhu W (2014) Modified precipitation processes and optimized copper content of $CuO\text{-}CeO_2$ catalysts for water-gas shift reaction. Int J Hydrogen Enengy 39:19570–19582
40. Chinchen G-C, Spencer M-S, Waugh K-C, Whan D-A (1987) Promotion of methanol synthesis and the water-gas shift reactions by adsorbed oxygen on supported copper catalysts. J Chem Soc Faraday Trans I 83:2193–2212
41. Sheffer G-R, King T-S (1989) Differences in the promotional effect of the group IA elements on unsupported copper catalysts for carbon monoxide hydrogenation. J Catal 116:488–497
42. Van Santen, R-A., Van Leeuwen, P.W.N.M., Moulijn, J-A., Averill, B-A. Catalysis: an integrated Approach Chapter 5: p218 (1997)
43. Yu J-F, Yang M, Zhang J-X, Ge Q-J, Zimina A, Pruessmann T, Zheng L, Grunwaldt J-D, Sun J (2020) Stabilizing Cu^+ in Cu/SiO_2 catalysts with a shattuckite-like structure boosts CO_2 hydrogenation into methanol. ACS Catal 10:14694–14706
44. Cui Y-Y, Dai W-L (2016) Support and morphology and crystal plane effect of Cu/CeO_2 nanomaterial on the physicochemical and catalytic properties for carbonate hydrogenation. Catal Sci Technol 6:7752–7762
45. Khobragade R, Roškarič M, Zerjav G et al (2021) Exploring the effect of morphology and surface properties of nanoshaped Pd/CeO_2 catalysts on CO_2 hydrogenation to methanol. Appl Catal A 627:118394
46. Sharma S-K, Paul B, Pal R-S, Bhanja P, Banerjee A, Samanta C, Bal R (2021) Influence of indium as a promoter on the stability and selectivity of the nanocrystalline Cu/CeO_2 catalyst for CO_2 hydrogenation to methanol. ACS Appl Mater Inter 13:28201–28213
47. Choi E-J, Lee Y-H, Lee D-W, Moon D-J, Lee K-Y (2017) Hydrogenation of CO_2 to methanol over $Pd\text{-}Cu/CeO_2$ catalysts. Mol Catal 434:146–153
48. Vourros A, Garagounis I, Kyriakou V, Carabineiro S-A-C, Maldonado-Hodar F-J, MarnellosG-E Konsolakis M (2017) Carbon dioxide hydrogenation over supported Au nanoparticles: effect of the support. J CO2 Util 19:247–256
49. Fan L, Fujimoto K (1993) Development of active and stable ceria supported palladium catalyst for hydrogenation of carbon dioxide to methanol. Appl Catal A 106:L1–L7